Use of micro computed-tomography and 3D printing for reverse engineering of mouse embryo nasal capsule

2016 JINST 11 C03006

(http://iopscience.iop.org/1748-0221/11/03/C03006)

Published by IOP Publishing for Sissa Medialab
Received: *December 7, 2015*
Accepted: *January 7, 2016*
Published: *March 2, 2016*

International workshop on Imaging
7–10 September 2015
Varenna, Italy

Use of micro computed-tomography and 3D printing for reverse engineering of mouse embryo nasal capsule

M. Tesařová,[a,b] T. Zikmund,[a] M. Kaucká,[c,d] I. Adameyko,[c,d] J. Jaroš,[e,f] D. Paloušek,[b] D. Škaroupka[b] and J. Kaiser[a,b,1]

[a] *CEITEC — BUT, Brno University of Technology, Technická 3058/10, 616 00 Brno, Czech Republic*
[b] *Faculty of Mechanical Engineering, Brno University of Technology, Technická 2896/2, 616 69 Brno, Czech Republic*
[c] *Department of Physiology and Pharmacology, Karolinska Institutet, Nanna Svartz väg 2, Stockholm 17177, Sweden*
[d] *Department of Molecular Neurosciences, Center for Brain Research, Medical University of Vienna, Spitalgasse 4, Vienna 1090, Austria*
[e] *Department of Histology and Embryology, Faculty of Medicine, Masaryk University, Kamenice 3, 625 00 Brno, Czech Republic*
[f] *International Clinical Research Center — Center of Biomolecular and Cellular Engineering, St. Anne's University Hospital Brno, Pekařská 53, 656 91, Brno, Czech Republic*

E-mail: jozef.kaiser@ceitec.vutbr.cz

Abstract: Imaging of increasingly complex cartilage in vertebrate embryos is one of the key tasks of developmental biology. This is especially important to study shape-organizing processes during initial skeletal formation and growth. Advanced imaging techniques that are reflecting biological needs give a powerful impulse to push the boundaries of biological visualization. Recently, techniques for contrasting tissues and organs have improved considerably, extending traditional 2D imaging approaches to 3D. X-ray micro computed tomography (μCT), which allows 3D imaging of biological objects including their internal structures with a resolution in the micrometer range, in combination with contrasting techniques seems to be the most suitable approach for non-destructive imaging of embryonic developing cartilage. Despite there are many software-based ways for visualization of 3D data sets, having a real solid model of the studied object might give novel opportunities to fully understand the shape-organizing processes in the developing body. In this feasibility study we demonstrated the full procedure of creating a real 3D object of mouse embryo nasal capsule, i.e. the staining, the μCT scanning combined by the advanced data processing and the 3D printing.

Keywords: Computerized Tomography (CT) and Computed Radiography (CR); Image reconstruction in medical imaging; Multi-modality systems

[1]Corresponding author.

doi:10.1088/1748-0221/11/03/C03006

2016 JINST 11 C03006

Contents

2016 JINST 11 C03006

1 Introduction

Despite the long-standing investigation of craniofacial development, this process is still not fully understood [1]. It is partially because of significant complexity of the structures in the head. These structures play an important role for vital functions through the whole life. The primary research of craniofacial development is often done on mouse embryos [2, 3]. Differences between the samples are usually investigated at craniofacial parts. Typical size of the mouse embryo nasal capsule at day 15 of embryonic development is in the range of few millimetres. There is a wide variety between different developmental stages or mutations that are manifested by small differences in the shape or thickness of the nasal capsule. In order to compare these fine details, high-resolution imaging techniques are needed.

For decades imaging has relied on optical and then also on electron microscopy of histological sections, which provides high resolution 2D data. Over time confocal microscopy enabled collection of optical sections through thicker samples [4]. Episcopic fluorescence image capturing is another technology for generating high-resolution 3D datasets. This method is based on capturing the autofluorescence of each of the histological slices. However, all above mentioned technologies are costly and time-consuming [5]. Optical projection tomography [6] is another approach for 3D imaging, but it is rather limited by sample size. The same accounts for light sheet microscopy (SPIM). Moreover, the sample preparation is rather complicated. Magnetic resonance imaging (MRI) currently represents an universal tool for different needs of soft tissue morphology [7]. This method uses magnetic field and radio waves in order to map various internal structures. MRI is suitable for imaging soft tissues such as internal organs, but it does not provide sufficient resolution for cartilage imaging [5].

One of the most convenient tools for imaging mouse embryonic samples from 12 to 17 days of embryonic development is X-ray computed tomography [3]. It is the oldest tomography imaging technique [8]. X-ray micro computed-tomography (μCT), i.e. X-ray computed-tomography with high spatial-resolution down to 1 μm, has the same principle as CT machines used for medical scanning. The sample that is placed between the X-ray source and the detector is rotated by 360° around its axis perpendicular to the line connecting the source and the detector. In every rotation step a two dimensional projection is taken. The sequence of obtained projections is subsequently processed by tomographic reconstruction based on inverse Radon transform [8]. In this way different X-ray absorption at each sample point is visualized and the 3D volume map of object density is created. Due to the cone shape of the X-ray beam, geometric magnification can be used to reach high-resolution [8].

X-ray tomography imaging has been limited by low contrast of soft un-mineralized tissues. Phase contrast can be the solution for enhancement of image quality of the X-ray projections [9]. However, this method is not much convenient for industrial and laboratory μCTs, where the image reconstruction rely predominantly on absorption contrast. Phase contrast is more applicable for monochromatic radiation used at synchrotrons [9, 10]. In the case of lab-based μCT systems it is necessary to use contrasting agents for increasing X-ray absorption of soft tissues. There are various methods that are using contrasting agents for staining of biological samples [11]. Phosphotungstic acid (PTA) was utilized as standard histological technique for light and electron microscopy due to its capability to increase the contrast of soft versus mineralized tissues or different type of soft tissues [12–14]. PTA also confers strong X-ray contrast when attached to the collagens and fibrils [12, 13], and to various other proteins. It is considered to be suitable for visualizing soft connective tissue in general [15]. Here we found that cartilage is stained significantly weaker in comparison to surrounding tissue, therefore we took the advantage of that for discriminating and outlining cartilage in μCT analysis.

Another step important for successful μCT is the mounting of the biological sample. It is crucial to have the sample fixed appropriately during the μCT scanning. Even a minuscule movement destroys the tomographic measurement and results in artefacts in the reconstructed tomographic cross-sections. It happens if samples are floating in aqueous or alcohol surrounding. Minimization of background can be reached by mounting the samples to hydrogels based on agarose, gelatine or alginate and by mechanical fixation of samples in standard laboratory equipment, like plastic tubes or polyimide tubes that are not very contrasting for X-rays.

If the contrast is sufficient, it is straightforward to visualize the 3D volume rendering of different features of the sample using proper tomographic software. The differentiation of these features is simply based on setting the appropriate gray values or gray value intervals in image histogram. However, it is difficult to set threshold for cartilage. As it was mentioned above, the cartilage is stained significantly weaker in comparison with surrounding tissue, so only its border is detectable (figure 1). In this case, data processing cannot be fully automated yet, but using suitable software tools enable relatively fast and precise manual segmentation of the craniofacial cartilage.

Here we present the whole process of reverse engineering of mouse embryo nasal capsule including staining and tomographic measurement combined with the advanced data processing for creating 3D model and its printing.

2016 JINST 11 C03006

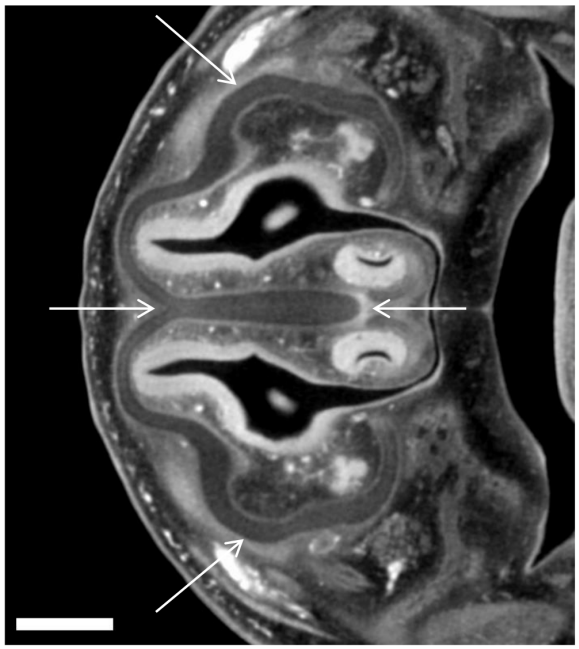

Figure 1. Reconstructed tomographic cross section of mouse embryo. Arrows show cartilage of nasal capsule. The length of the scale bar is 0.4 mm.

2 Materials and methods

2.1 Preparation of samples for micro CT measurements, staining

Our staining protocol has been modified from protocol developed by Brian Metscher [15]. After excision, the 15.5 days old C57BL strain mouse embryos were fixed with 4% formaldehyde in phosphate buffer saline (PBS) for 24 hours at +4°C. Samples were then washed with PBS and dehydrated by ethanol grade (30%, 50%, 70%), each concentration for 1 day.

We experimentally found out the best tissue contrast and penetration with PTA (10026-AP0, Lach-Ner, Czech Republic) dissolved in 90% methanol (21190-11000, Ing. Petr Švec-PENTA, Czech Republic). Therefore we transferred the samples from 70% ethanol (71250-11000, Ing. Petr Švec-PENTA, Czech Republic) to ethanol-methanol-water mixture (4:4:3) and then into 80% and 90% methanol, each bath for 1 hour. After that, 0.7% PTA-methanol solution was used to stain the samples for 6 days and exchanged every day with the fresh one.

The staining was followed by rehydration of the samples in methanol grade series (90%, 80%, 70%, 50% and 30%) to end up in sterile distilled water. After that, rehydrated embryos were embedded in 0.5% agarose gel (A5304, Sigma-Aldrich) and placed in 1.5 ml polypropylene tubes to avoid the movement artefacts during X-ray computer tomography scanning.

2.2 CT measurement and gathering data for 3D printing

The polypropylene tube was fixed on a plastic rod by a silicone gun. The rod was mounted in the chuck which provides the position of the sample in rotation axis (figure 2). The μCT scanning was performed using laboratory system GE Phoenix v|tome|x L 240 (GE Sensing & Inspection

2016 JINST 11 C03006

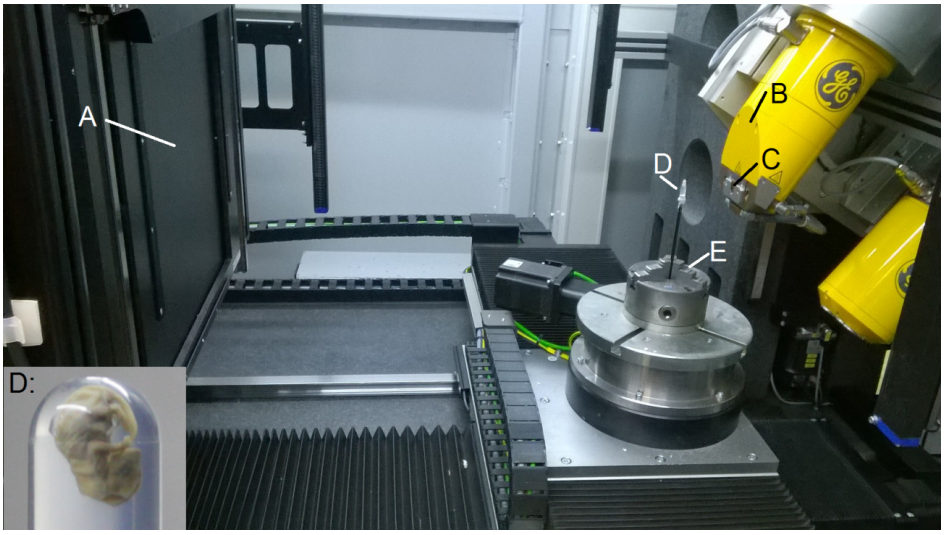

Figure 2. Fixing the sample for μCT measurement. A — flat panel detector; B — X-ray tube; C — aluminium filter; D — embryo embedded in agarose gel in the tube; E — chuck.

Technologies GmbH, Germany), equipped with a 180 kV/15 W maximum power nanofocus X-ray tube and high contrast flat panel detector DXR250 with 2048×2048 pixel^2, 200×200 μm^2 pixel size. The exposure time was 900 ms in every of the 2200 positions. The utilized acceleration voltage and X-ray tube current were 60 kV and 200 μA, respectively. The beam was filtered by the beryllium window of the X-ray housing and by 0.2 mm of aluminium filter. The voxel size of obtained volume was 5 μm. The tomographic reconstruction was realized using 3D computed tomography software GE phoenix datos|x 2.0 (GE Sensing & Inspection Technologies GmbH, Germany). The data processing was realized in software VG Studio MAX 2.2 (Volume Graphics GmbH, Germany). Segmentation of nasal capsule was completed manually (approx. 8 hours of segmentation). The "smoothing" tool, with strength 20 was used to smooth the virtual 3D model in order to get rid of inaccuracies.

2.3 Additive manufacturing — 3D printing

The Parts have been manufactured by ZPrinter 650 (Peak Solutions, U.S.A.). Building volume is $254 \times 381 \times 203$ mm and layer thickness was established to 0.1016 mm. Color printing resolution in x and y directions is 600×540 dots per inch (DPI) and the minimum feature size is also 0.1016 mm. All data were adjusted in the 3D printing software ZPrint 7.15 (Peak Solutions, U.S.A.).

The STL data generated from μCT measurements were scaled 50 times directly in the 3D printing software. Monochromatic green color, the same color that was used as a virtual color in VG studio MAX 2.2 software, was chosen. The printer spread 716 layers of plaster based powder, where each layer was bound by five Hewlett Packard print heads (CMYK binders + one Clear binder) with the resolution of 600×540 DPI. After 6 hours and 15 minutes the printing was finished and the printer dried up the part still surrounded by the powder in the building chamber. Dry part was carefully removed from the powder by vacuumer and brush and depowdered by compressed air in the post-processing unit. It was infiltrated by cyanoacrylate using drizzle method to give it additional strength, durability, and color vibrancy.

2016 JINST 11 C03006

Figure 3. The obtained data from the μCT measurement. The cross section in two perpendicular planes and the 3D render of the whole 15.5 days old embryo. The length of the scale bar is 3 mm.

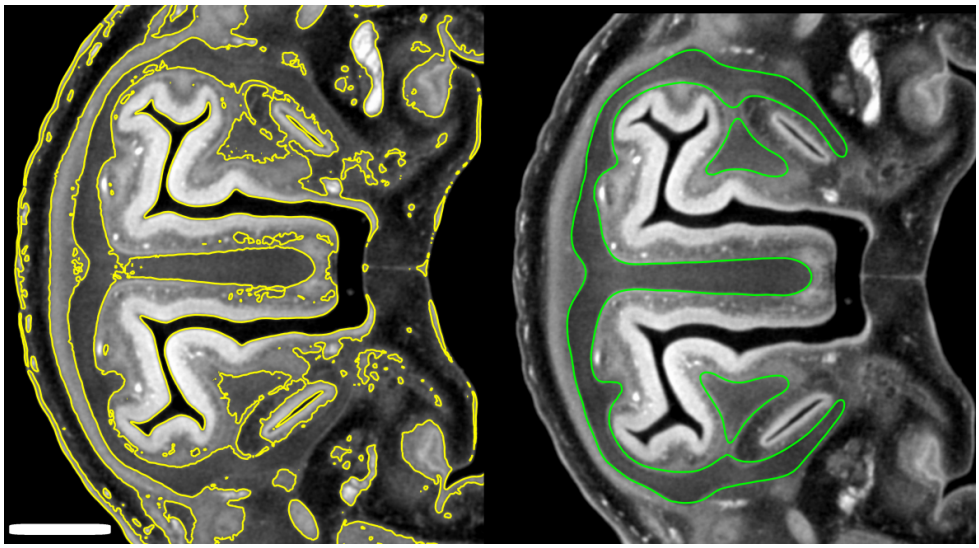

Figure 4. Comparison between automatic (yellow) and manual (green) segmentation. The length of the scale bar is 0.5 mm.

3 Results

The overall procedure is demonstrated on a representative 15.5 days old mouse embryo stained by PTA. The μCT measurement had a satisfactory contrast for the overall 3D render of the mouse embryo (figure 3).

Gray value intervals for border of the cartilage was not sufficiently pronounced for automatic segmentation (figure 4). The manual segmentation was realized in one direction across the sample, along the cross section shown in figures 1 and 5, denoted x, y in figure 5. Using manual segmentation, a 3D model of a nasal capsule was created (figure 6).

2016 JINST 11 C03006

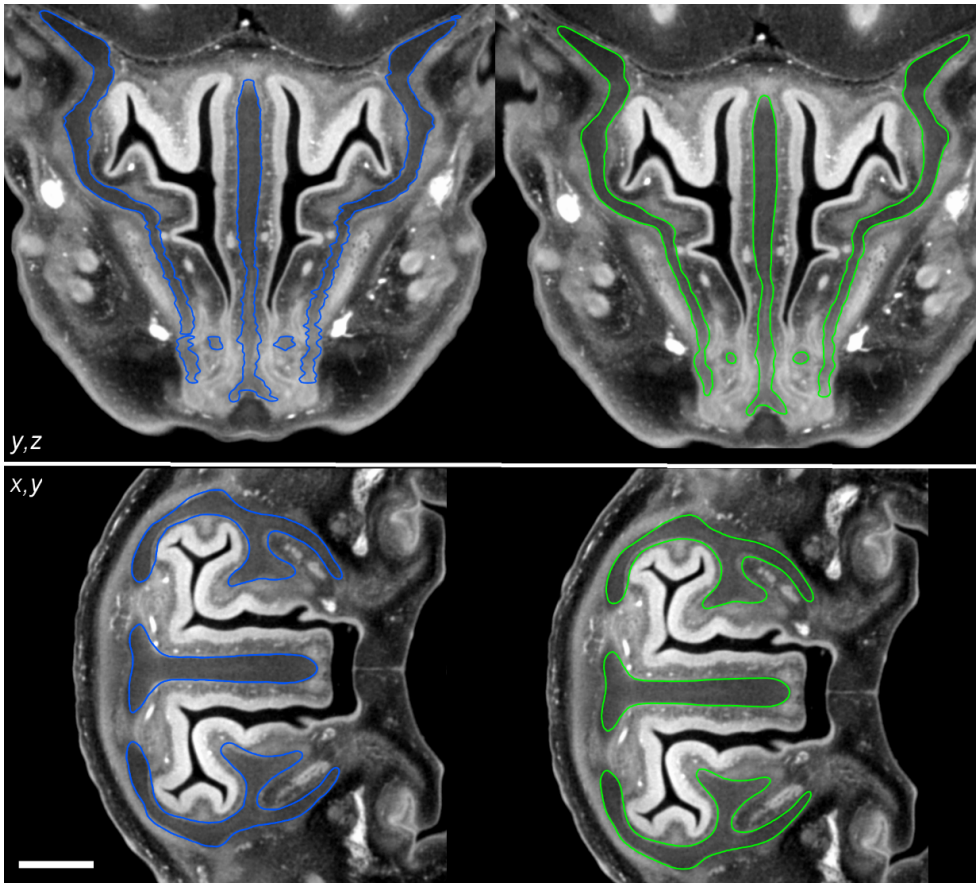

Figure 5. Using the "smoothing" tool. Blue line — before the application of the tool, green line — after the smoothing. The upper part shows the cross section y, z, perpendicular to the cross section x, y in which the segmentation was realized. The smoothing was controlled in the cross section x, y (bottom image) by comparing the segmented and smoothed data. The length of the scale bar is 0.35 mm.

Segmentation along one cross section caused disfluencies in the perpendicular cross section y, z (figure 5). After the segmentation these visible distinct inaccuracies were smoothed and fluent model was obtained. The smoothing parameter was optimized that way to preserve the small details. This was controlled by comparison with the original tomographic cross sections x, y (figure 5 and 6).

The finished virtual 3D model was exported to STL format for 3D printing. The printed 3D model is compared with the STL model in figure 7.

Figure 8 shows the comparison of the printed 3D model of an olfactory system with the human hand.

4 Discussions and ongoing work

Even if the proper combination of different techniques may represent a breakthrough with clinical significance, the use of advanced techniques in multi-disciplinary biological research is nowadays still a challenge [16]. Using μCT, stereolitography computer-aided design (STL CAD) modeling and matrix-assisted laser desorption-ionisation — time of flight mass spectrometry (MALDI-TOF

2016 JINST 11 C03006

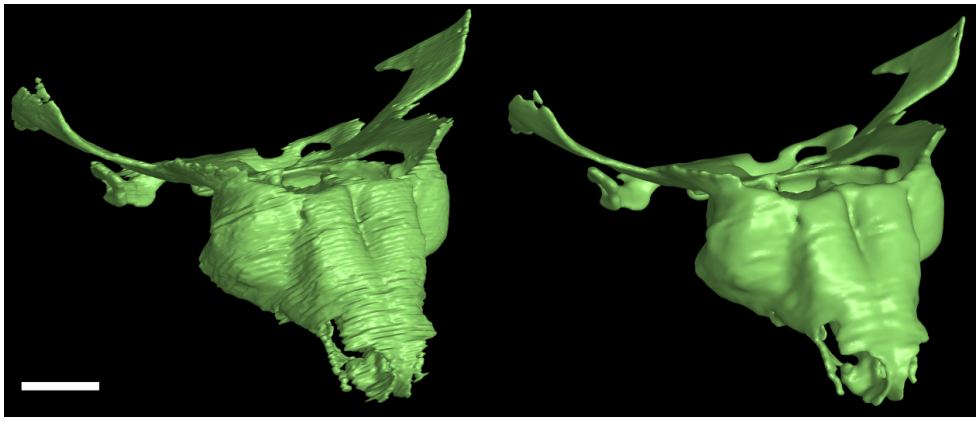

Figure 6. Segmented models without smoothing (left) and with smoothing (right). The length of the scale bar is 0.5 mm.

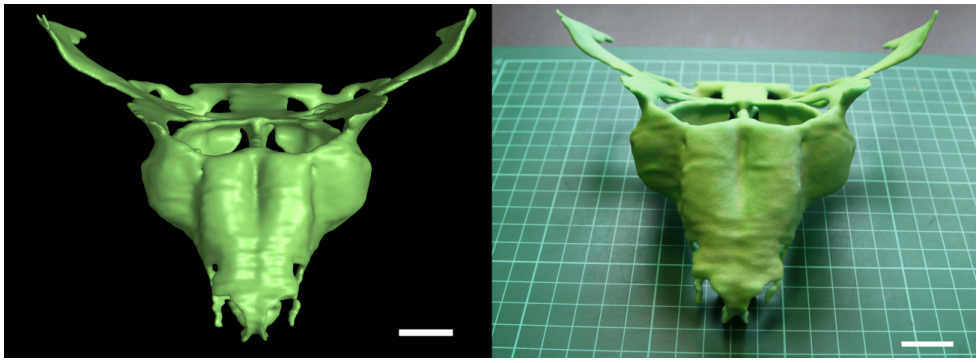

Figure 7. Comparison of the STL model (left) with the 50:1 upscaled model from 3D print (right). The scale bar is 0.4 mm (left) and 2 cm (right).

Figure 8. Comparison of the object from 3D print with human hand.

2016 JINST 11 C03006

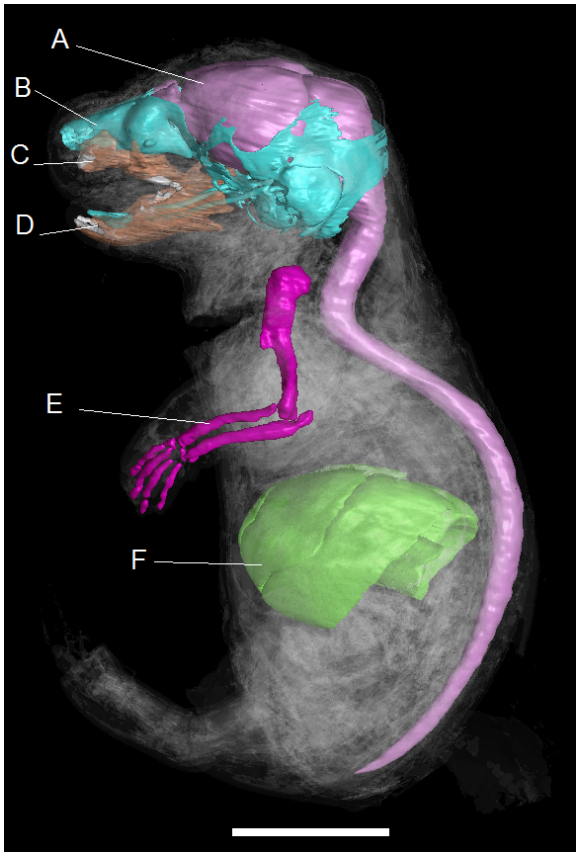

Figure 9. Segmented parts of 17.5 days old mouse embryo by using μCT. A — brain with spinal cord; B — cranium; C — upper jaw; D — lower jaw; E — upper limb; F — liver. The length of the scale bar is 4 mm.

MS) we recently confirmed the causative role of absorbable suture material in the pathogenesis of hollow channel structures in some canine compound uroliths [17]. The straightforward combination of μCT with 3D printing is however more common in medical practice [18–20]. In [18] the medical uses of 3D printing are reviewed, with the main emphasis on surgical training, special surgical planning and prosthetics applications. The overview of the main requirements for medical imaging affected needs of additive manufacturing (AM) formerly known as rapid prototyping is reviewed in [19]. It is shown that successful clinical cases of AM rely heavily in multi-disciplinary approach, i.e. on efficient collaboration between various disciplines, as operating surgeons, radiologists and engineers. The review also intends to narrow the potential communication gap between radiologists and engineers who work with projects involving AM by showcasing the overlap between the two disciplines. The possibilities to apply 3D printers in veterinary medicine are explored and illustrated in review [20]. It is stated that the increased use of this technology in human medicine together with the decreasing cost are making 3D printing more affordable also for veterinary use.

Combining the μCT imaging, and 3D printing with tissue staining, the possibilities of reverse engineering are very broad. Here we created the real 3D cartilage model of the 15.5 days old mouse embryo to show that these techniques are suitable for demonstrating the complexity of biological structures (figure 9).

2016 JINST 11 C03006

Using 3D printers, the physical exploration is extending observation of the samples by viewing from all sides, sensing surface roughness and wall thickness. Simple visualization of images on a computer does not allow all of these qualities for research, demonstrations and educational purposes.

Definitely, it is not easy to orient in such sophisticated geometry using only imagination even empowered by visualizing software. Researchers also may focus on developmental shape transformations of spine, limbs etc. The inner ear with its complex structure could be another part of the cartilaginous tissue suitable for such reverse engineering.

With sufficient resolution allowing the segmentation, one μCT scan lasts about 2 hours. The relatively short scanning time gives an opportunity for creating entire real anatomical atlases or databases allowing researchers to browse in different structures, mutants etc. In addition, after one scan, objects can be printed in different scales or colors, which can also be used for educational purposes [18]. 3D print is a rapidly evolving technology and several methods exists like STL, digital light processing (DLP), laser sintering and laser melting, extrusion of thermoplastic material etc. Using this technology it is affordable to make such a collection.

μCT also enables to display another soft tissues — liver, heart, gray matter i.e. brain and spinal cord (figure 7). μCT so can complete other techniques that can image 3D structures (e.g. MRI, optical projection tomography [18] or high resolution episcopic microscopy). Using the specific advantages of each of these methods a complex and sophisticated 3D structure can be visualized and subsequently printed on 3D printers.

5 Conclusions

Here we have demonstrated the comprehensive process of the reverse engineering of mouse embryo nasal capsule. For this feasibility study a 15.5 days old mouse embryo was chosen as a representative sample that was contrasted by phosphotungstic acid. It was shown that the combination of micro computed-tomography with 3D printing brings new possibilities for exploring and understanding the processes in craniofacial development. Combination of these two methods can be also useful for various studies in developmental, comparative and quantitative biology.

Acknowledgments

This work is an output of cooperation between CEITEC — Central European Institute of Technology (CZ.1.05/1.1.00/02.0068) and NETME Centre, regional R&D centre built with the financial support from the Operational Programme Research and Development for Innovations within the project NETME Centre (New Technologies for Mechanical Engineering), Reg. No. CZ.1.05/2.1.00/01.0002 and, in the follow-up sustainability stage, supported through NETME CENTRE PLUS (LO1202) by financial means from the Ministry of Education, Youth and Sports under the National Sustainability Programme I. JJ acknowledge the support by FNUSA-ICRC Project (No. CZ.1.05/1.1.00/02.0123) from the European Regional Development Fund. JK acknowledge the support of Brno University of Technology on the frame of grant FSI-S-14-2494 (Application of Advanced Optical Methods). MK was supported by EMBO long-term fellowship.

2016 JINST 11 C03006

References

[1] B. Hallgrímsson, D.E. Lieberman, W. Liu, A.F. Ford-Hutchinson and F.R. Jirik, *Epigenetic interactions and the structure of phenotypic variation in the cranium*, *Evol. Dev.* **9** (2007) 76.

[2] T.E. Parsons et al., *Phenotypic variability and craniofacial dysmorphology: increased shape variance in a mouse model for cleft lip*, *J. Anat.* **212** (2008) 135.

[3] K. Degenhardt, A.C. Wright, D. Horng, A. Padmanabhan and J.A. Epstein, *Rapid 3D phenotyping of cardiovascular development in mouse embryos by micro-CT with iodine staining*, *Circ. Cardiovasc. Imaging* **3** (2010) 314.

[4] W.J. Weninger et al., *High-resolution episcopic microscopy: a rapid technic for high detailed 3D analysis of gene activity in the context of tissue architecture and morphology*, *Anat. Embryol.* **211** (2006) 213.

[5] F.C. Norris et al., *A coming of age: advanced imaging technologies for characterising the developing mouse*, *Trends Genet.* **29** (2013) 700.

[6] J. Kerwin et al., *3 dimensional modelling of early human brain development using optical projection tomography*, *BMC Neurosci.* **5** (2004) 27.

[7] S.W. Ruffins et al., *Digital three-dimensional atlas of quail development using high-resolution MRI*, *Sci. W. J.* **7** (2007) 592.

[8] W.A. Kalender, *Computed tomography: fundamentals, system technology, image, quality, applications*, 3rd edition, Wiley (2005).

[9] J. Kaiser et al., *Investigation of the microstructure and mineralogical composition of urinary calculi fragments by synchrotron radiation X-ray microtomography: a feasibility study*, *Urol. Res.* **39** (2011) 259.

[10] E. Eggl et al., *X-ray phase-contrast tomography with a compact laser-driven synchrotron source*, *Proc. Natl. Acad. Sci. USA* **112** (2015) 5567.

[11] B.D. Metscher, *Micro-CT for comparative morphology: simple staining methods allow high contrast 3D imaging of diverse non-mineralized animal tissues*, *BMC Phys.* **9** (2009) 11.

[12] V.S. Constantine and R.W. Mowry, *Selective staining of human dermal collagen*, *J. Inv. Derm.* **50** (1968) 419.

[13] T. Nemetschek, H. Riedl and R. Jonak, *Topochemistry of the binding of phosphotungstic acid to collagen*, *J. Mol. Biol.* **133** (1979) 67.

[14] R.N. Rao, P.M. Fallman, D. Greer Falls and S.N. Meloan, *A comparative study of PAS-phosphotungstic acid-Diamine Supra Blue FGL and immunological reactions for type I collagen*, *Histochemistry* **91** (1989) 283.

[15] B.D. Metscher, *MicroCT for developmental biology: a versatile tool for high-contrast 3D imaging at histological resolutions*, *Dev. Dynam.* **238** (2009) 632.

[16] H.G. Elmendorf and A.G. Rosenwald, *Biology of global health: preparing students for multi-disciplinary group work*, in Proceedings of the *2014 ASCB/IFCB Meeting*, Philadelphia U.S.A., 6–10 Dec 2014.

[17] J. Kaiser et al., *Determination of the cause of selected canine urolith formation by advanced analytical methods*, *J. Small Anim. Pract.* **53** (2012) 646.

2016 JINST 11 C03006

[18] F. Rengier et al., *3D printing based on imaging data: review of medical applications*, *Int. J. Comput. Assist. Radiol. Surg.* **5** (2010) 335.

[19] E. Huotilainen et al., *Imaging requirements for medical applications of additive manufacturing*, *Acta Radiol.* **55** (2014) 78.

[20] A.M. Hespel, R. Wilhite and J. Hudson, *Applications for 3D printers in veterinary medicine*, *Vet. Radiol. Ultrasoun.* **55** (2014) 347.

2016 JINST 11 C03006